Journal of Microscopy, Vol. 214, Pt 3 June 2004, pp. 287–296
Received 28 October 2003; accepted 19 December 2003

Off-axis electron holography of electrostatic potentials in unbiased and reverse biased focused ion beam milled semiconductor devices

A. C. TWITCHETT, R. E. DUNIN-BORKOWSKI, R. J. HALLIFAX, R. F. BROOM & P. A. MIDGLEY
Department of Materials Science and Metallurgy, University of Cambridge, Pembroke Street, Cambridge CB2 3QZ, U.K.

Key words. Electrostatic potential, focused ion beam milling, off-axis electron holography, p-n junction.

Summary

Off-axis electron holography in the transmission electron microscope (TEM) is used to measure two-dimensional electrostatic potentials in both unbiased and reverse biased silicon specimens that each contain a single *p–n* junction. All the specimens are prepared for examination in the TEM using focused ion beam (FIB) milling. The *in situ* electrical biasing experiments make use of a novel specimen geometry, which is based on a combination of cleaving and FIB milling. The design and construction of an electrical biasing holder are described, and the effects of TEM specimen preparation on the electrostatic potential in the specimen, as well as on fringing fields beyond the specimen surface, are assessed.

Introduction

Off-axis electron holography is a promising technique for the characterization of electrostatic potentials in doped semiconductor devices in the transmission electron microscope (TEM) (e.g. Rau *et al.*, 1999; Gribelyuk *et al.*, 2002). The technique, which is illustrated schematically in Fig. 1(a) and described in detail elsewhere (e.g. Midgley, 2001; Lehmann & Lichte, 2002; Dunin-Borkowski *et al.*, 2004), relies on the use of an electrostatic biprism to overlap an electron wave that has passed through the specimen with another part of the same electron wave that has passed only through vacuum. If a coherent field emission electron source is used, then the overlap region contains interference fringes whose local intensity and spacing can be used to measure the amplitude and the phase shift of the electron wave, respectively. The phase shift ϕ is of particular interest for the characterization of semiconductor devices as it provides access to the electrostatic potential in the specimen (integrated in the electron beam direction), which is related to the distribution of electrically active dopant atoms. For a non-magnetic specimen, ϕ can be described by the equation

$$\phi(x,y) = C_E \int V(x,y,z)\,\mathrm{d}z \qquad (1)$$

where V is the electrostatic potential seen by the beam, z is a direction parallel to, and x and y are directions perpendicular to, the incident electron beam. C_E is a specimen-independent constant that takes a value of 7.3×10^6 rad V^{-1} m^{-1} at a microscope accelerating voltage of 200 kV. If the potential V does not change along z inside a specimen of thickness t, then Eq. (1) can be simplified to

$$\phi(x,y) = C_E V(x,y) t(x,y). \qquad (2)$$

The primary contributions to $V(x,y)$ in a doped semiconductor are the mean inner potential V_0 (which is related to the composition and density of the specimen and takes a value of ~12 V for silicon), the space charge (or dopant) potential (which results from changes in doping concentration) and electrostatic fringing fields outside the specimen surface.

A two-dimensional map of the phase shift across the specimen recorded using electron holography reveals *n*- and *p*-type regions directly as areas of bright and dark contrast, respectively. Equation (2) can be used to relate the phase shift across each such *p–n* junction to the built-in voltage across the junction V_{bi} if the specimen thickness is known. This capability is of great interest to the semiconductor industry, which has a pressing need for high spatial resolution information about dopant profiles for the evaluation of process parameters, and as input to simulations of dopant diffusion. However, it is increasingly recognized that TEM specimen preparation

Correspondence to: Dr Rafal Dunin-Borkowski. Fax: +44 (0)1223 334563; e-mail: red10@cam.ac.uk

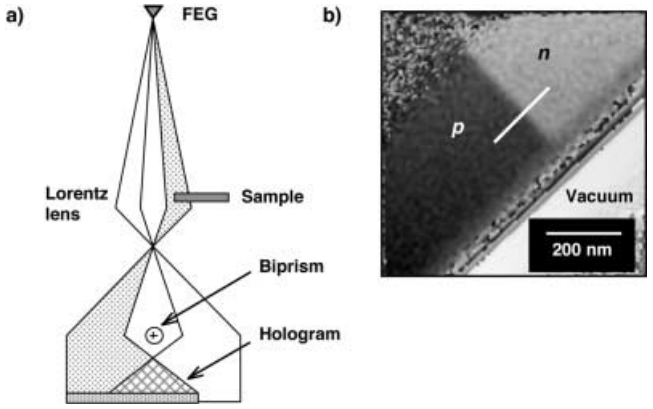

Fig. 1. (a) Schematic diagram showing the set-up required for off-axis electron holography. The field emission gun (FEG) provides a coherent source of electrons. The Lorentz lens allows an optimal field of view and holographic interference fringe spacing for acquiring holograms of semiconductor devices to be obtained. A positive voltage is applied to the biprism wire to form the hologram, which is recorded digitally. (b) Representative phase image reconstructed from an off-axis electron hologram of the Si *p–n* junction sample. The sample edge is at the lower right of the image, and no attempt has been made to remove the phase 'wraps' lying along this edge. The white line shows the region from which phase profiles such as those shown in Fig. 8 were obtained.

can have a significant effect on the electron holographic phase shift measured from a doped semiconductor, and can alter the potential in the specimen from that in the original device. It is therefore important to develop and to assess the effect of different specimen preparation techniques on dopant potentials measured using electron holography.

The technique of focused ion beam (FIB) milling, which typically involves using a 30-kV gallium ion beam to micromachine a specimen to electron transparency, is of particular interest as it is increasingly used to prepare site-specific regions of semiconductor devices for electron holography (e.g. Wang *et al.*, 2002a,b; Donnet *et al.*, 2003). Specimen preparation using FIB milling has an advantage over more conventional approaches that involve mechanical polishing and ion milling or cleaving, in that an optimal, uniform specimen thickness for electron holography of 200–500 nm can be achieved with relative ease. This optimal thickness allows the electron holographic phase change to be maximized without reducing the fringe contrast substantially (Rau *et al.*, 1999). FIB milling is also unique in its site-specificity, unlike either tripod polishing (McCartney *et al.*, 2002) or cleaving (Hetherington, 1988; Walck & McCaffrey, 1997) and allows a region of vacuum for a reference wave to be machined close to the area of interest. However, physical damage, and both implantation and doping of the specimen surface with gallium (Ishitani *et al.*, 1998; McCaffrey *et al.*, 2001), may result in the modification of the electronic properties of the doped region and must be minimized if the technique is to be used to quantify the properties of the device reliably and reproducibly. Strain, unwanted variations in local specimen thickness and specimen charging (e.g. McCartney *et al.*, 2002) may also result from specimen preparation using techniques such as FIB milling, particularly if a device contains areas of metallization or heterogeneous interfaces. The structures on the surface of a semiconductor device that are required to provide electrical isolation and contacts to the doped regions may also need to be removed to overlap the vacuum reference wave with the wavefront passing through the area of interest.

In this paper, we outline some experimental aspects of the application of off-axis electron holography to silicon *p–n* junction specimens that have been prepared for the TEM using FIB milling, and which have no additional complications from surface metallization or passivation layers. We compare results obtained using two distinct specimen geometries, one of which allows the *p–n* junction to be biased electrically *in situ* in the TEM. In order to apply a voltage across an FIB-milled specimen, we describe a specimen preparation procedure that allows two electrical contacts to be applied to the sample. In addition to the benefit of examining a 'working' semiconductor device in the TEM, a further advantage of subjecting a specimen to an applied electrical bias is that unwanted contributions to the contrast from thickness variations and strain can, in principle, be removed by taking the difference between electron holographic phase images recorded with different voltages applied to the specimen. Some of the results presented here have been presented in preliminary form elsewhere (Twitchett *et al.*, 2002).

Experimental details

The silicon *p–n* junction examined in this study comprised a 2.5-μm-thick boron-doped *p*-type layer, which had been grown directly on to an antimony-doped *n*-type substrate using molecular beam epitaxy. The dopant concentration on each side of the junction was nominally in excess of 10^{18} cm^{-3}, corresponding to a predicted built-in voltage V_{bi} of ~0.9 V and a predicted total depletion width W of ~50 nm. Figure 1(b) shows a representative electron holographic phase image obtained from an unbiased FIB-milled specimen of the *p–n* junction, recorded from a specimen of crystalline thickness 410 nm (see below), whereas Fig. 2 shows a secondary ion mass spectrometry (SIMS) profile obtained from the device. The parameters V_{bi} and W are defined in Fig. 3. In all of the experiments described below, specimens were tilted from the <100> zone axis to a weakly diffracting orientation in order to ensure that contributions to the contrast from dynamical diffraction were minimized, while keeping the *p–n* junction edge-on to better than 0.2°.

Phase images were reconstructed from off-axis electron holograms that had been acquired using a Philips CM300 field emission gun (FEG) TEM equipped with a Super-Twin objective lens, an additional high-strength Lorentz minilens,

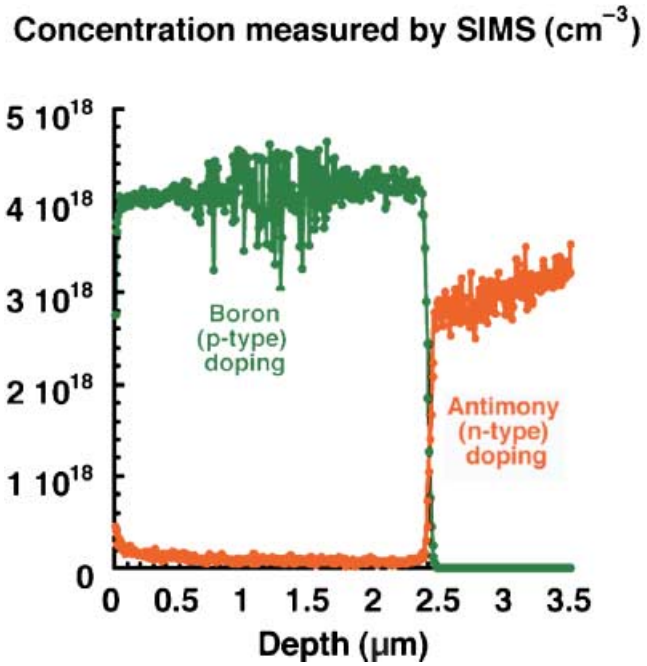

Fig. 2. Secondary ion mass spectrometry (SIMS) profile obtained from the sample examined in this study, which contains a single *p–n* junction at a depth of 2.5 μm below the wafer surface.

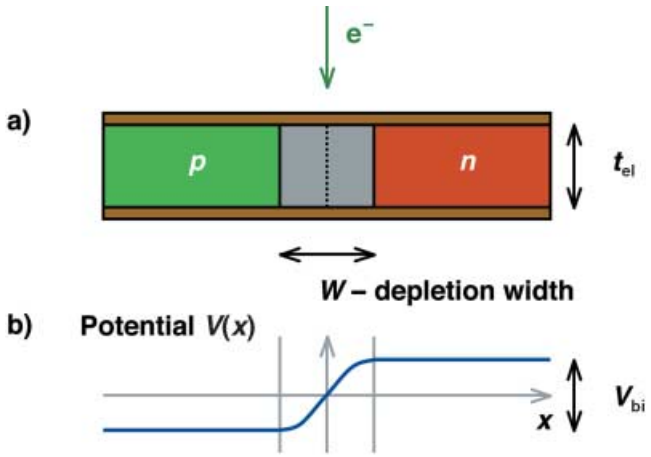

Fig. 3. (a) Schematic diagram showing the cross-sectional geometry of a TEM specimen of uniform thickness that contains a symmetrical semiconductor *p–n* junction. t_{el} is the 'electrically active' sample thickness. The layers at the top and bottom surfaces of the specimen represent electrically passivated or depleted layers, whose physical and electrical nature is affected by TEM specimen preparation. (b) Schematic diagram showing the electrostatic potential profile across the *p–n* junction. V_{bi} is the built-in voltage, while W is the width of the depletion region over which the potential changes. The sign convention for the potential is consistent with the mean inner potential of the specimen being positive relative to vacuum.

and a rotatable Möllenstedt-Düker biprism (a gold-coated quartz fibre). The microscope was operated at an accelerating voltage of 200 kV (rather than at 300 kV) in order to minimize the effects of knock-on damage on the silicon specimen. The use of a Lorentz lens instead of the conventional microscope objective lens, combined with a further increase in the strength of the diffraction lens, allowed an optimal overlap region (hologram field of view) on the specimen of 0.5–0.8 μm to be achieved at a biprism voltage of 70–100 V. The interference fringe spacing was then 5–10 nm, and the holographic fringe contrast was ~25%. Holograms were acquired digitally on a 2048-pixel charge-coupled device (CCD) camera, which was located at the end of a Gatan Imaging Filter (GIF) 2000, using acquisition times of between 4 and 16 s. All of the image analysis required to recover the phase and amplitude of the electron wave from the recorded electron holograms (e.g. Völkl & Lehmann, 1999), and all subsequent image processing, were carried out using library programs written in the Semper image processing system (Saxton *et al.*, 1979). The phase shift in each image was evaluated modulo 2π and subsequently 'phase unwrapped'. In Fig. 1(b), phase unwrapping has been carried out everywhere except at the specimen–vacuum interface, where the specimen thickness changes rapidly. In this phase image, a grey band, visible along the specimen edge, may be indicative of the presence of a depleted, passivated or damaged surface layer, which is seen directly in cross-section in this image but is thought to encompass the entire sample surface. Such phase images can be compared with the predicted electrostatic potential $V(x)$ across an abrupt *p–n* junction, which is shown schematically in Fig. 3 (Sze, 2002). In Fig. 3(a), the effect of the unknown electrical state of the specimen surface on the potential is included phenomenologically by assuming the presence of electrically 'dead' layers of total thickness t_{dead} on the specimen surfaces. The true junction potential is then assumed to lie within a specimen thickness t_{el}, which is smaller than the total specimen thickness $t = t_{el} + t_{dead}$.

Specimen preparation

Standard FIB milling in 'trench' geometry (e.g. Langford & Petford-Long, 2001), which is illustrated schematically in Fig. 4(a,b), was carried out in an FEI 200 FIB workstation for holographic experiments that did not involve applying a bias to the junction *in situ* in the TEM. Regions of six different thicknesses were prepared in two adjacent 'windows' on a single TEM specimen. Each region of interest was protected from gallium implantation and damage by depositing a protective platinum strap on to the original wafer surface, using a low ion current of 150 pA to minimize the damage caused to the top wafer surface. A high ion current of 11.5 nA was used initially to mill the trenches. This current was reduced to 150 pA for the final milling of the membrane surfaces. As a result of the relatively large distance of 2.5 μm between the wafer surface and the junction, additional FIB cuts were made in each membrane using a beam current of 150 pA, as shown

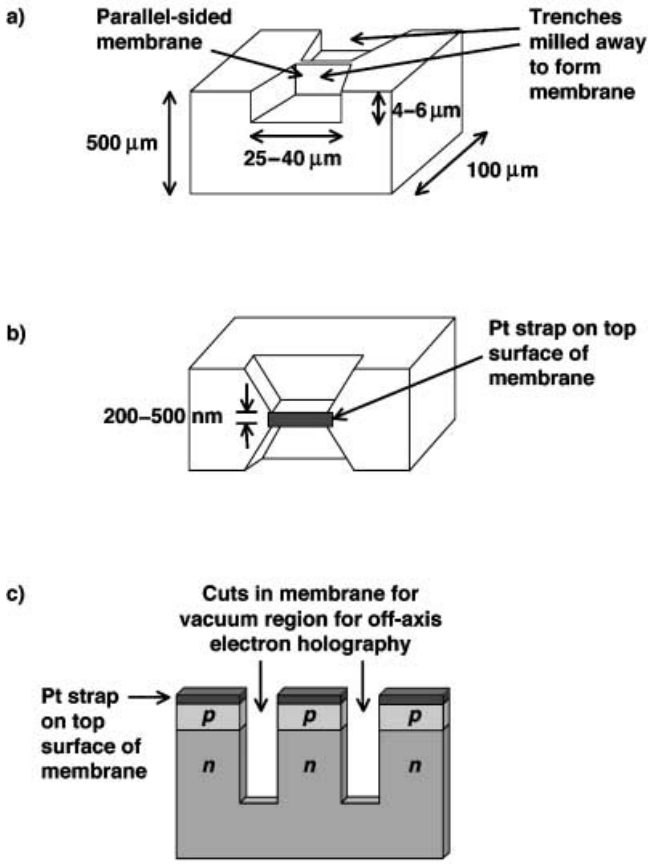

Fig. 4. (a) Schematic diagram showing the conventional 'trench' focused ion beam milling approach used to prepare a specimen of a *p–n* junction for examination by electron holography. This specimen geometry is not used for electrical biasing experiments in the present study. (b) Alternative view of the same specimen geometry, showing the Pt strap deposited on the semiconductor surface to protect it from the Ga ion beam. (c) Schematic diagram showing the final cuts to the membrane, which are required to provide a vacuum reference wave close to the region of interest for off-axis electron holography.

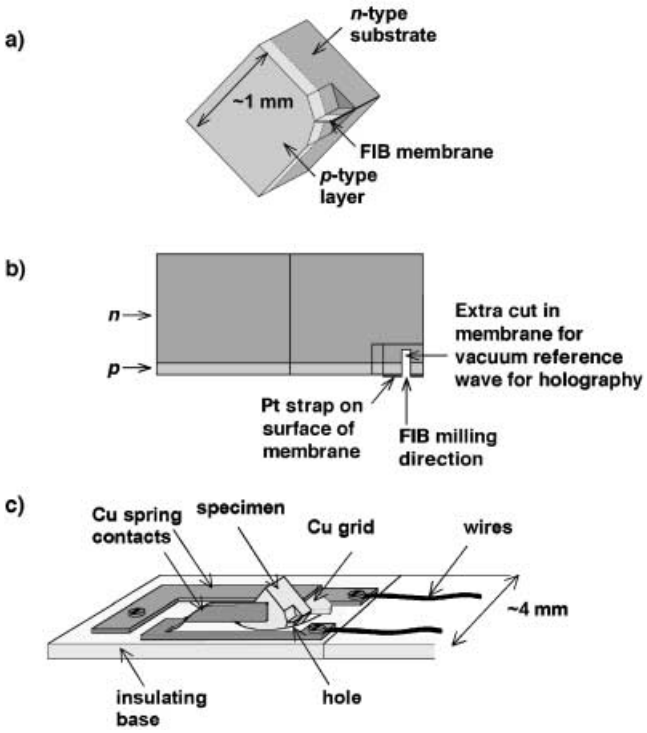

Fig. 5. (a) Schematic diagram showing the specimen geometry used for electrical biasing experiments in the present study. The specimen is prepared by cleaving a 1–2-mm square of wafer, one corner of which is subsequently focused ion beam milled parallel to the original wafer growth direction. (b) Schematic diagram (not to scale) showing the Pt strap and the extra cut, made by focused ion beam milling, for the vacuum reference wave required for off-axis electron holography. (c) Schematic diagram showing the home-built electrical biasing holder used in the present study, with the specimen in place. The specimen is glued to the edge of a Cu grid using conducting epoxy, and then clamped between two spring contacts on an insulating base.

schematically in Fig. 4(c), to provide a vacuum reference near the *p–n* junction for off-axis electron holography. The specimen was placed in a standard double tilt holder for electron holography. All holograms were reconstructed with the aid of reference holograms, which were acquired from vacuum immediately after each hologram of the specimen to remove geometric distortions associated with the imaging and recording process (de Ruijter & Weiss, 1993).

An alternative specimen geometry, also based on FIB milling and illustrated in Fig. 5(a,b), was developed to examine the same *p–n* junction under an applied electrical bias. Electrically biased semiconductor junctions have been examined previously by Titchmarsh *et al.* (1969) and Pozzi (1979) using Foucault and Fresnel imaging, and using off-axis electron holography by Frabboni *et al.* (1985). However, these experiments were carried out on specimens in which the thickness varied rapidly, and quantitative analysis of the phase shifts in the interior of the specimen was not performed. Our approach involved cleaving (in air) a 1–2-mm square of wafer, which contained the *p–n* junction and had been polished from the substrate side to a thickness of ~50 μm. FIB milling was then carried out on one corner of the square to provide a parallel-sided membrane of uniform thickness in a specimen that was robust enough to handle, and which could be clamped between two spring contacts in order to apply a bias across the junction in the TEM. *In situ* biasing experiments were then carried out using a two-contact electrical biasing holder, which was modified from a conventional Philips heating holder that had two internal wires to link the specimen to external contacts. The design of the holder is shown schematically in Fig. 5(c). Modification of this holder involved manufacturing a new end-piece that allowed the specimen to be securely clamped whilst isolating the electrical contacts to it from the main body of the holder. The end piece contained a printed circuit board (PCB), on to which copper tracks were patterned to provide electrical contacts between the incoming wires and

the specimen. The PCB provided electrical isolation between the main body of the holder and the biasing circuit. The original substrate side of the cleaved wafer was glued on to the thin straight edge of a solid semicircle of copper, using conducting silver epoxy to provide an electrical contact through the copper to the back (*n*-type) side of the wafer. This semicircle was then clamped on to a copper track that had been patterned on to the PCB, which had a drilled hole through which electrons could pass. A second spring contact was applied to the original front surface of the wafer. A beryllium–copper spring was used to clamp the specimen into the holder, pressing the specimen grid on to one contact. The second contact was made by pressing the face of the cleaved wedge against a beryllium–copper spring, as shown in Fig. 5(c). One of the electrical contacts to the semiconductor junction was earthed to provide a path for the dissipation of charge in the specimen generated by the electron beam, and reverse bias voltages of up to 3 V were applied to the sample. Severe charging of the sample when illuminated by the electron beam was eliminated by sputtering gold on to the back-side of the PCB. A copper spring was also inserted to improve the electrical contact between the PCB and the body of the holder, and the hole for the electron beam was coated with silver without compromising the electrical isolation of the circuit containing the device. Photographs showing the upper and lower sides of the biasing holder, with a specimen clamped between the two copper spring contacts, are shown in Fig. 6(a,b), respectively. The conducting silver paint around the hole for the electron beam in the PCB is visible in Fig. 6(b).

Whichever specimen preparation approach was used, great care was taken during FIB milling to ensure that the focused gallium ions were only directed parallel to the surfaces of the thin membrane. In this way, gallium implantation was minimized, although not excluded completely. The current of the gallium beam used to form the final membrane was 150 pA with a probe (full width at half maximum) of 10 nm. No further specimen preparation was undertaken before examination in the TEM. As no metallic contacts were present on the wafer surface, the specimens did not show any local strain or thickness variations ('curtaining').

Two-beam convergent beam electron diffraction (CBED) patterns were used to provide accurate (±5%) measurements of the crystalline thicknesses of the membranes (Williams & Carter, 1996). The unbiased membrane thicknesses were determined to be 220, 270 and 410 nm, and the crystalline thickness of the biased membrane was 390 nm.

Figure 7 shows experimental phase images of a cleaved 90° wedge that had not been FIB milled, obtained under an applied reverse bias. In this specimen, the thickness increases rapidly, and the variation in electrostatic potential can only be revealed in the vacuum region outside the position of the *p*–*n* junction. The montage of images in Fig. 7 shows the four-times-amplified cosine of the measured electron holographic

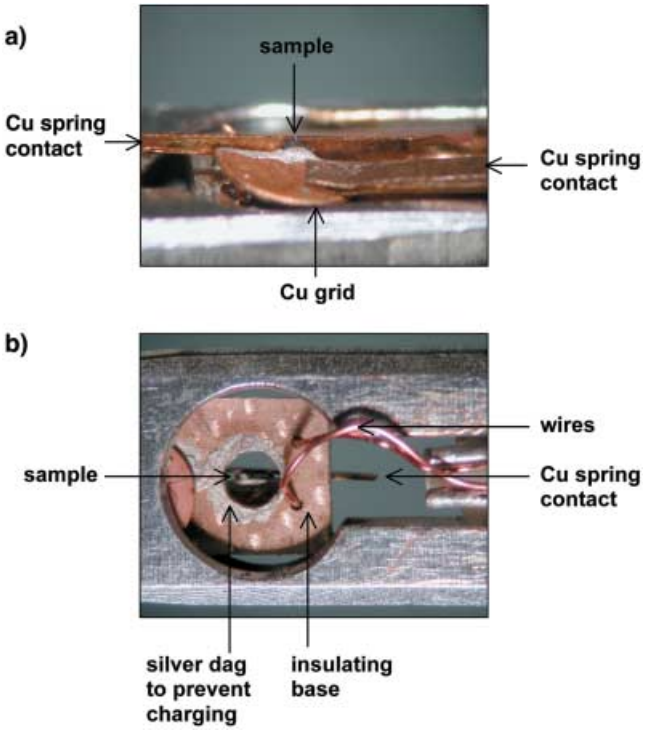

Fig. 6. Annotated photographs showing a *p*–*n* junction specimen in the biasing holder, viewed from (a) above and (b) below. The semicircular Cu grid shown in (a) has a diameter of 3 mm.

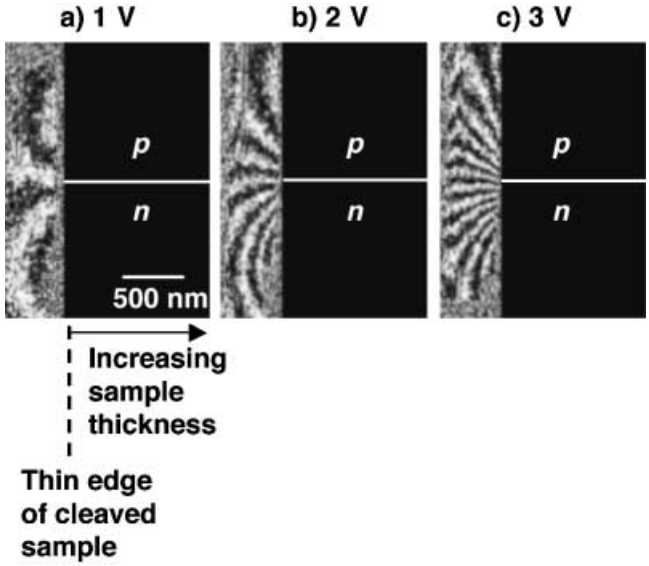

Fig. 7. Four-times-amplified cosine of the measured phase, showing the electrostatic fringing field in the vacuum region outside the position of the *p*–*n* junction in a 90° cleaved wedge that had not been FIB milled, for the three different applied reverse bias voltages indicated. The zero bias hologram was used as the reference hologram when forming each phase image. The phase shift inside the present specimen, whose thickness increases rapidly, could not be reconstructed successfully.

phase shift for three different reverse bias voltages applied to the cleaved specimen. An external fringing field that increases in strength with applied reverse bias is visible at the position of the *p–n* junction. Although such fringing fields were never observed outside specimens that had been FIB milled, these phase images, which were reconstructed using the 0-V hologram as a reference hologram, provide preliminary confirmation that the experimental set-up illustrated in Figs 5 and 6 can be used to vary the bias applied to the *p–n* junction in the TEM. Images such as those shown in Fig. 7 can only be interpreted quantitatively by comparing them with simulations as both the object and the reference waves contributing to the interference pattern are affected by the long-range, three-dimensional external fields (Matteucci *et al.*, 1998).

Experimental results

All the phase images acquired from the FIB-prepared membranes revealed the position of the *p–n* junction. The corresponding amplitude images showed no measurable change in contrast at the junction, indicating that the measured phase changes were associated primarily with the change in dopant concentration, and not with diffraction contrast or specimen thickness variations.

Holograms that had been acquired using the biasing holder were reconstructed using either a standard vacuum reference hologram to remove geometrical distortions, or using the zero bias hologram as the reference hologram. The latter approach resulted in a 'difference' image, revealing only phase changes arising from the applied electrical bias. In contrast to results from cleaved specimens (Fig. 7), phase images of the *p–n* junction never revealed detectable fringing fields outside the FIB-milled specimens, either with or without an applied bias. This observation is in agreement with the results of Frabboni *et al.* (1985), and suggests that the surfaces of FIB-milled specimens are always equipotentials, even when subject to an applied bias.

Figure 8 shows examples of line profiles across the *p–n* junction obtained directly from the recorded phase images. The line profiles were averaged parallel to the junction over a distance of 100 nm, both for three unbiased specimens (Fig. 8a) and for four reverse bias voltages applied to a single specimen (Fig. 8b). All of the profiles agree qualitatively with the expected variation in potential across the junction shown schematically in Fig. 3(a), and the step in phase, $\Delta\phi$, increases as expected with both specimen thickness and reverse bias voltage according to the equation

$$\Delta\phi = C_E(V_{bi} + V_{appl})t_{el} \equiv C_E(V_{bi} + V_{appl})(t - t_{dead}) \qquad (3)$$

where V_{bi} is the built-in voltage across the *p–n* junction, V_{appl} is the applied reverse bias voltage, and t, t_{el} and t_{dead} are the total, electrically active and electrically inactive contributions to the specimen thickness, respectively.

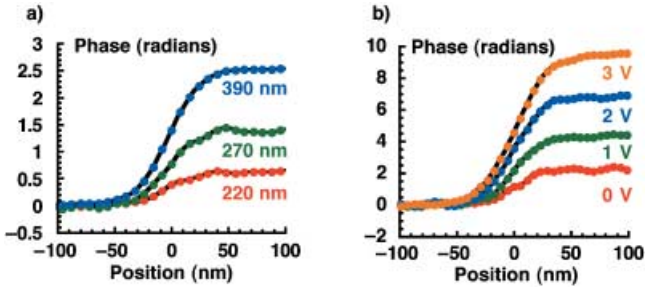

Fig. 8. Line profiles of the measured phase shift across the Si *p–n* junction, shown as a function of (a) specimen thickness for three different unbiased focused ion beam milled 'trench' specimens, and (b) reverse bias voltage for a single sample whose crystalline thickness was measured to be 390 nm. The phase images were averaged over a distance of approximately 100 nm across the specimen in order to form the profiles, in which the zero of phase has been chosen to lie on the left (the *p*-) side of the junction.

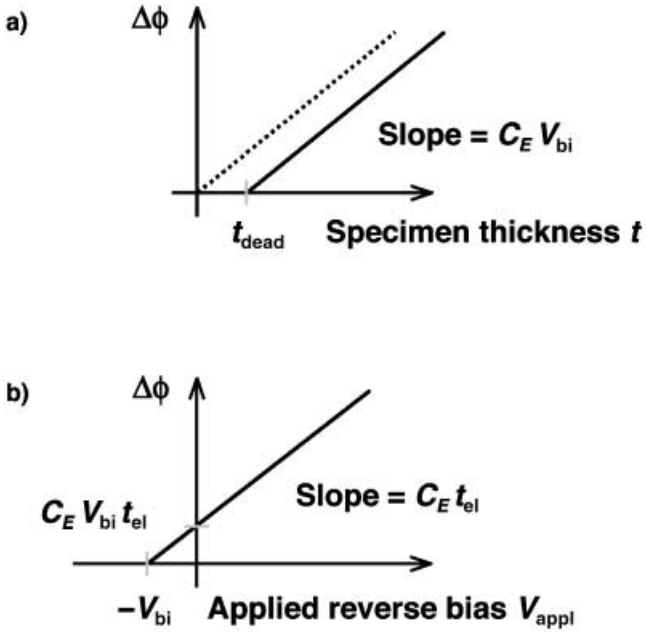

Fig. 9. Schematic diagrams showing graphs of the step in phase $\Delta\phi$ across a *p–n* junction expected as a function of (a) the total specimen thickness, and (b) the reverse bias applied across the TEM specimen.

Examination of Eq. (3) suggests that it should be possible to use a plot of $\Delta\phi$ against t to measure V_{bi} from its slope and t_{dead} from its intercept with the horizontal axis, as illustrated schematically in Fig. 9(a). Similarly, a plot of $\Delta\phi$ against V_{appl} should allow t_{el} to be determined from its slope and V_{bi} from its intercept with the horizontal axis, as illustrated schematically in Fig. 9(b). Figure 10 shows experimental measurements of $\Delta\phi$ plotted as a function of the measured crystalline contribution to the specimen thickness t_{cr} for the unbiased 'trench' FIB-milled specimens. The intercept of the data points with the horizontal axis should provide the crystalline contribution

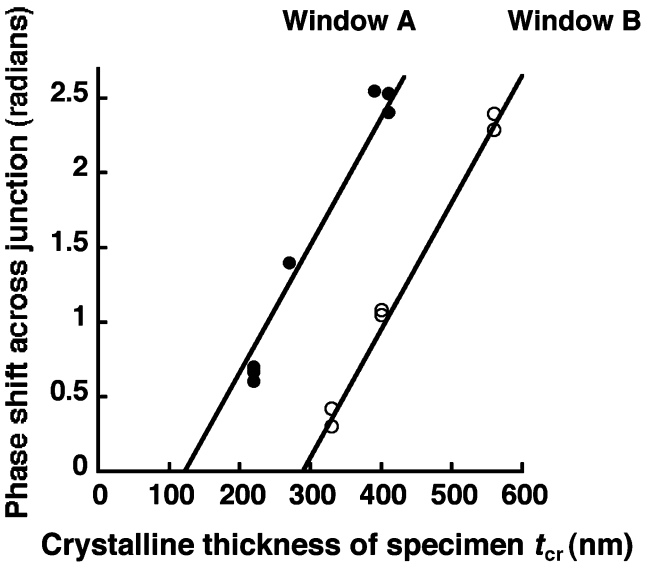

Fig. 10. The step in phase $\Delta\phi$ across the *p–n* junction examined in this study, measured from off-axis electron holograms of several membranes of different thickness in an unbiased 'trench' specimen. The solid circles were obtained from membranes in window A, and show results obtained after taking great care to ensure that the specimen was focused ion beam milled only at a glancing angle to the surface of the thin membrane. The open circles were obtained from membranes in window B, which may have been implanted with additional gallium.

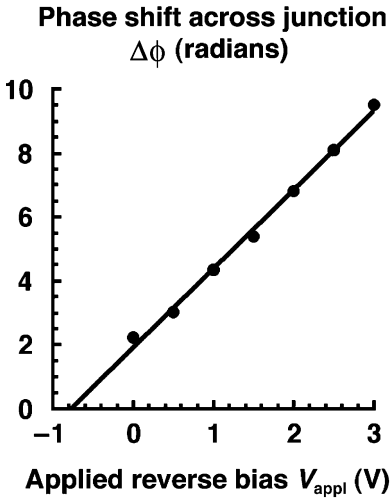

Fig. 11. The experimentally measured step in phase $\Delta\phi$ across the *p–n* junction examined in this study, measured as a function of applied reverse bias voltage from off-axis electron holograms of a single focused ion beam milled specimen whose crystalline thickness was measured to be 390 nm.

to the electrically 'dead' layer thickness. Unexpectedly, two distinct lines are obtained from windows A and B in the 'trench' specimen, with intercepts close to 100 and 300 nm, respectively. The difference between these results may arise from the exposure of window B to the gallium ion beam during FIB milling of window A, at a time when there was no protective platinum deposited over this area. If this interpretation is correct, then it confirms the sensitivity of the crystalline part of the electrically inactive layer thickness to gallium implantation. An alternative explanation may involve the redeposition of material during FIB milling. This result highlights the importance of establishing a standard FIB specimen preparation routine in order to ensure reproducible results.

Figure 11 shows a similar plot of the phase change $\Delta\phi$ across the *p–n* junction as a function of applied reverse bias. This graph is important as its linearity and slope set limits for the minimum potential that has been dropped across the *p–n* junction. On the assumption that the magnitude of V_{bi} is unchanged with reverse bias, and that the applied voltage is dropped entirely across the junction, the gradient of the graph in Fig. 11 provides a lower limit for t_{el} of 335 ± 5 nm for a specimen whose crystalline thickness is 390 nm, suggesting that an upper limit for the thickness of the electrically 'dead' crystalline layers on each surface of the specimen is 28 ± 5 nm. This dead layer, if present, is in addition to the layer of amorphized material on the specimen surfaces. Lattice disorder arising from Ga ion implantation may result in the Fermi energy being close to the mid-gap in this region (Nguyen & O'Leary, 2000). The value of V_{bi} measured from Fig. 11 is 0.9 ± 0.1 V. It should be noted that V_{bi} is far more difficult to measure accurately from the gradients of the graphs shown in Fig. 10 than from the plot in Fig. 11 as variations in 'dead' layer thickness between different specimens introduce additional errors.

Additional insight into the nature of the surface of the FIB-milled specimens can be obtained by measuring the thickness of the (electrically 'inactive') amorphous layers on the specimen surfaces. Figure 12 shows a measure of the total (crystalline plus amorphous) specimen thickness $t(x,y)$ obtained, in units of inelastic mean free path λ_{in}, from each holographic amplitude image $A(x,y)$ (after normalizing by the amplitude of the reference image) by using the equation

$$\frac{t(x,y)}{\lambda_{in}} = -2 \ln A(x,y) \qquad (4)$$

(Gajdardziska-Josifovska & McCartney, 1994). Although the value of λ_{in} obtained using this equation is strictly a weighted average of that in the crystalline region of the sample and in the amorphous overlayers on its surfaces, these values are expected to be similar here as any amorphous layers are likely to be formed from damaged (or oxidized) silicon. The total thickness of the amorphous material is determined to be 50 ± 20 nm from the intercept of the graph with the horizontal axis, suggesting the presence of an amorphous overlayer whose average thickness is 25 ± 10 nm on each surface of the specimen. This amorphous layer could result from damage or sputtering during specimen preparation, from native oxide formation on the exposed silicon surfaces, or from carbon contamination within the microscope.

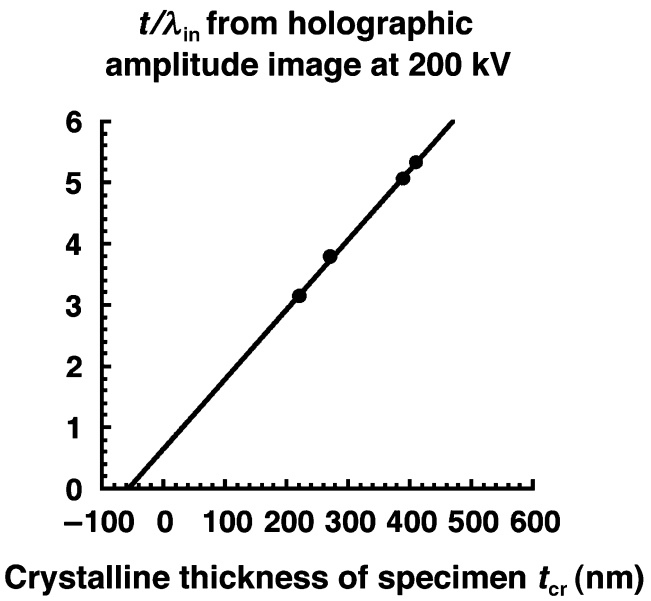

Fig. 12. Specimen thickness t in units of inelastic mean free path λ_{in}, obtained from holographic amplitude images and plotted as a function of the crystalline specimen thickness measured using convergent beam electron diffraction. The slope of the graph indicates that $\lambda_{in} = 85$ nm for crystalline Si at a microscope accelerating voltage of 200 kV. The intercept of the graph on the horizontal axis suggests that ~50 nm of the total specimen thickness (~25 nm on each surface) is amorphous.

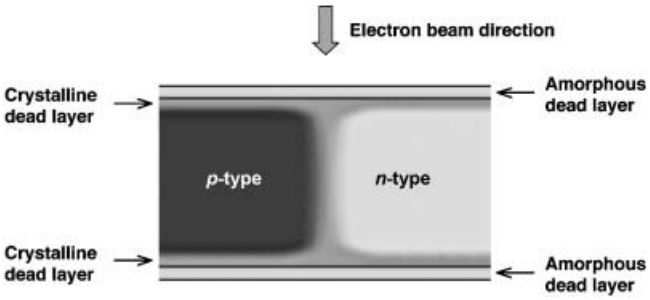

Fig. 13. Schematic diagram showing, in cross-section, the physical and electrical structure of a focused ion beam milled TEM specimen inferred from the present study.

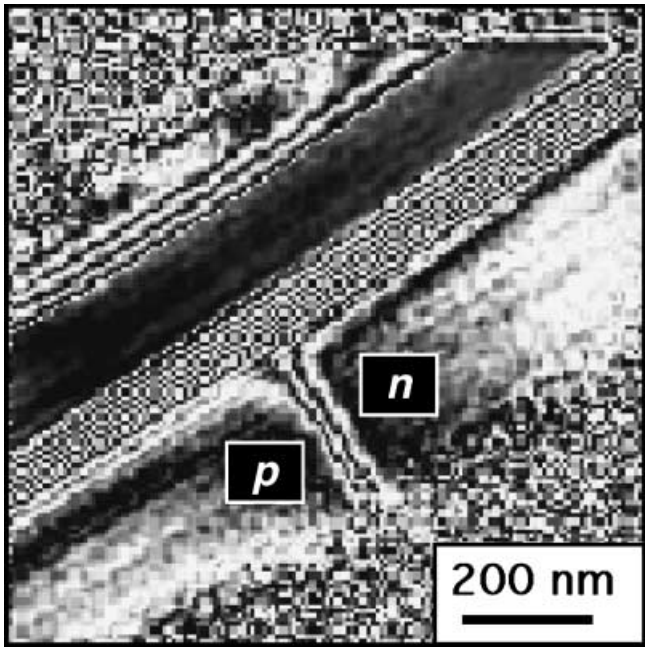

Fig. 14. Four-times-amplified cosine of the measured phase acquired from a focused ion beam milled specimen at a reverse bias voltage of 3 V, reconstructed using the zero volt bias image as a reference hologram. Note the absence of electrostatic fringing fields in the vacuum region outside the specimen edge.

Our results, which are consistent between unbiased specimens and specimens to which electrical contacts (but no voltage) were applied, suggest that a layered structure may be present in the TEM membrane, with amorphous outer surface layers surrounding inner, crystalline electrically dead surface layers, themselves surrounding the crystalline electrically active material, as shown schematically in Fig. 13. At the surface of a semiconductor, a region that is depleted of charge carriers can be formed as a result of band-bending effects (e.g. Sze, 2002). An associated increase in the depletion width of the *p*–*n* junction arises in the region near the surface (see also Fig. 14 below). The electrically dead, crystalline layer inferred from the biased results can be thought of as a *p*–*n* junction with an infinite depletion width. Accordingly, the schematic diagram in Fig. 13 shows the depletion width varying with depth in the membrane, approaching infinity at the top and bottom surfaces of the electrically active region.

The fact that the surface of an FIB milled specimen is an equipotential is illustrated in Fig. 14, which shows a reconstructed phase image, amplified four times, as in Fig. 7 for the cleaved wedge sample. The electrostatic potential at the specimen edge, close to the position of the *p*–*n* junction, is different between the *p*- and *n*-doped regions, changing more slowly with distance from the specimen edge on the *p* side. The vacuum region shows no variation in phase close to the position of the junction, confirming our previous observations that FIB specimen preparation results in a negligible external electrostatic potential variation.

The specimen surface layers were investigated further by collecting secondary electrons from the TEM sample in a field emission gun scanning electron microscope (FEGSEM) operated at an accelerating voltage of 1 kV. Both an FIB-prepared specimen and a cleaved wedge containing the *p*–*n* junction were examined. The contrast across the junction, which is shown in Fig. 15, was approximately five times lower for the FIB membrane than for the cleaved specimen. Although the mechanism of dopant contrast in the SEM is still not fully understood, the depth of measurement is known to be small compared with the membrane thickness, and therefore will

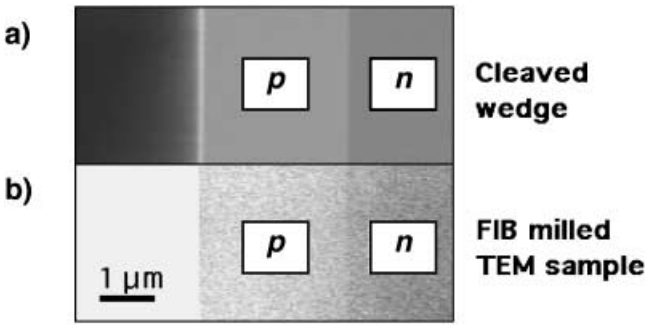

Fig. 15. Scanning electron microscope (SEM) images acquired by collecting secondary electrons from (a) a 90° cleaved wedge, and (b) a focused ion beam milled TEM membrane containing the Si *p–n* junction examined in this study.

probe only the surface layers. The fact that the surface of the FIB-prepared membrane shows a lower contrast indicates that the variation in potential close to the semiconductor surface is reduced compared with that in the cleaved specimen.

Discussion and conclusions

The use of off-axis electron holography to characterize the dopant potential across a silicon *p–n* junction prepared for TEM examination using FIB milling has been assessed. The internal electrostatic potential profile across the junction has been measured for both a standard FIB geometry and a geometry that allows *in situ* electrical biasing experiments to be performed in the TEM. Analysis of the results requires a number of assumptions, both because the built-in voltage V_{bi} cannot be separated from the electrically active specimen thickness t_{el} from a single electron hologram, and because the difference between the value of t_{el} on the *p* and the *n* sides of the junction is unknown. In the present study, we have assumed that the electrically 'dead' layer thickness is identical on both sides of the junction. Our results then show that the active region of the device is contained within the central part of the specimen, sandwiched between a crystalline electrically 'dead' layer whose thickness depends on gallium implantation and an additional amorphous surface overlayer. We speculate that the crystalline 'dead' layer may result from the presence of point defects, including vacancies and clusters of implanted gallium atoms. *In situ* electrical biasing experiments reveal a built-in voltage across the *p–n* junction of 0.9 ± 0.1 V. For unbiased specimens prepared using FIB milling, results obtained with and without electrical contacts to the active regions of the device are identical within experimental error. Although a technique such as small-angle cleaving may provide more quantitative results for the potential, electric field and charge density across the junction, the assessment and development of FIB milling for electron holographic studies is still essential owing to its unparalleled site-specificity. The benefits of applying an electrical bias *in situ* in the electron microscope have been demonstrated. However, the device examined here is relatively simple, and the examination of more complex devices may require a more advanced biasing holder and more complicated specimen preparation. It should be emphasized that phase profiles such as those shown in Fig. 8 are relatively insensitive to the precise form of the charge density profile across the *p–n* junction. The use of computer simulations to analyse the phase profiles shown in Fig. 8, and a comparison between the fitted charge densities with those expected from the SIMS profile shown in Fig. 2, are described elsewhere (Twitchett *et al.*, 2004).

Acknowledgements

We are grateful to Philips Research (Eindhoven) for the Si *p–n* junction specimen, Dr R. Hervig for the SIMS analysis, Dr C. Schonjahn for the SEM imaging, and the Royal Society, the EPSRC and Newnham College, Cambridge, for financial support.

References

Donnet, D.M., De Veirman, A.E.M., Otterloo, B. & Roberts, H. (2003) Novel FIB-TEM preparation methods for semiconductor device characterisation and failure analysis. *Inst. Phys. Conf. Ser.* **180**, 617–620.

Dunin-Borkowski, R.E., McCartney, M.R. & Smith, D.J. (2004) Electron holography of nanostructured materials. *Encyclopaedia of Nanoscience and Nanotechnology* (ed. by H. S. Nalwa). American Scientific Publishers, in press.

Frabboni, S., Matteucci, G., Pozzi, G. & Vanzi, M. (1985) Electron holographic observations of the electrostatic field associated with thin reverse-biased p-n junctions. *Phys. Rev. Lett.* **55**, 2196–2199.

Gajdardziska-Josifovska, M. & McCartney, M.R. (1994) Absolute measurement of normalised thickness t/1 from off-axis electron holography. *Ultramicroscopy*, **53**, 283–289.

Gribelyuk, M.A., McCartney, M.R., Li, J., Murthy, C.S., Ronsheim, P., Doris, B., McMurray, J.S., Hegde, S. & Smith, D.J. (2002) Mapping of electrostatic potential in deep submicron CMOS devices by electron holography. *Phys. Rev. Lett.* **89**, 5502–5505.

Hetherington, C. (1988) Preparation of semiconductor cross-sections by cleaving. *Mat. Res. Soc. Symp. Proc.*, **115**, 143–148.

Ishitani, T., Koike, H., Yaguchi, T. & Kamino, T. (1998) Implanted gallium-ion concentrations of focused-ion-beam prepared cross sections. *J. Vac. Sci. Technol.* **B16**, 1907–1913.

Langford, R.M. & Petford-Long, A.K. (2001) Preparation of transmission electron microscopy cross-section specimens using focused ion beam milling. *J. Vac. Sci. Technol.* **A19**, 2186–2193.

Lehmann, M. & Lichte, H. (2002) Tutorial on off-axis electron holography. *Microsc. Microanal.* **8**, 447–466.

Matteucci, G., Missiroli, G.F. & Pozzi, G. (1998) Electron holography of long-range electrostatic fields. *Adv. Imaging Electron Phys.* **99**, 171–240.

McCaffrey, J.P., Phaneuf, M.W. & Madsen, L.D. (2001) Surface damage formation during ion-beam thinning of sample for transmission electron microscopy. *Ultramicroscopy*, **87**, 97–104.

McCartney, M.R., Gribelyuk, M.A., Li, J., Ronsheim, P., McMurray, J.S. &

Smith, D.J. (2002) Quantitative analysis of one-dimensional dopant profile by electron holography. *Appl. Phys. Lett*. **80**, 3213–3216.

Midgley, P.A. (2001) An introduction to off-axis electron holography. *Micron*, **32**, 167–184.

Nguyen, T.H. & O'Leary, S.K. (2000) The dependence of the Fermi energy on temperature, doping concentration, and disorder in disordered semiconductors. *J. Appl. Phys*. **88**, 3479–3483.

Pozzi, G. (1979) On the interpretation of out-of-focus images of p–n junctions whose internal field topography is described by the one-sided step model. *Optik*, **53**, 381–394.

Rau, W.D., Schwander, P., Baumann, F.H., Hoppner, W. & Ourmazd, A. (1999) Two-dimensional mapping of the electrostatic potential in transistors by electron holography. *Phys. Rev. Lett*. **82**, 2614–2617.

de Ruijter, W.J. & Weiss, J.K. (1993) Detection limits in quantitative off-axis electron holography. *Ultramicroscopy*, **50**, 269–283.

Saxton, W.O., Pitt, T.J. & Horner, M. (1979) Digital image processing: the Semper system. *Ultramicrosocopy*, **4**, 343–354.

Sze, S.M. (2002) *Physics of Semiconductor Devices*. Wiley, New York.

Titchmarsh, J.M., Lapworth, A.J. & Booker, G.R. (1969) A new method for investigating the electric field regions of p-n junctions. *Phys. Stat. Solidi*, **34**, K83–K87.

Twitchett, A.C., Dunin-Borkowski, R.E., Hallifax, R.J., Broom, R.F. & Midgley, P.A. (2004) Off-axis electron holography of a reverse-biased focused ion beam milled Si *p-n* junction. *Microsc. Microanal*. in press.

Twitchett, A.C., Dunin-Borkowski, R.E. & Midgley, P.A. (2002) Quantitative electron holography of biased semiconductor devices. *Phys. Rev. Lett*. **88**, 238–302.

Völkl, E. & Lehmann, M. (1999) The reconstruction of off-axis electron holograms. *Introduction to Electron Holography* (ed. by E. Völkl, L. F. Allard and D. C. Joy), pp. 125–151. Plenum Press, New York.

Walck, S. & McCaffrey, J.P. (1997) The small angle cleavage technique: an update. *Mat. Res. Soc. Symp. Proc.* **480**, 149–171.

Wang, Z., Hirayama, T., Sasaki, K., Saka, H. & Kato, N. (2002a) Electron holographic characterisation of electrostatic potential distributions in a transistor sample fabricated by focused ion beam. *Appl. Phys. Lett*. **80**, 246–248.

Wang, Z., Kato, T., Shibata, N., Hirayama, T., Kato, N., Sasaki, K. & Saka, H. (2002b) Characterizing an implanted Si/Si p-n junction with lower doping level by combined electron holography and focused-ion-beam milling. *Appl. Phys. Lett*. **81**, 478–480.

Williams, D.B. & Carter, C.B. (1996) *Transmission Electron Microscopy: a Textbook for Materials Science*. Plenum Press, New York.